



## OPEN

SUBJECT AREAS:  
SOLAR CELLS  
APPLIED PHYSICSReceived  
6 May 2014Accepted  
4 August 2014Published  
22 August 2014Correspondence and  
requests for materials  
should be addressed to  
X.D.Z. (xdzhang@  
nankai.edu.cn)\* These authors  
contributed equally to  
this work.

# Two-dimensional high efficiency thin-film silicon solar cells with a lateral light trapping architecture

Jia Fang\*, Bofei Liu\*, Ying Zhao &amp; Xiaodan Zhang

Institute of Photo Electronics Thin Film Devices and Technology of Nankai University, Key Laboratory of Photoelectronic Thin Film Devices and Technology, Tianjin 300071, P. R. China.

Introducing light trapping structures into thin-film solar cells has the potential to enhance their solar energy harvesting as well as the performance of the cells; however, current strategies have been focused mainly on harvesting photons without considering the light re-escaping from cells in two-dimensional scales. The lateral out-coupled solar energy loss from the marginal areas of cells has reduced the electrical yield indeed. We therefore herein propose a lateral light trapping structure (LLTS) as a means of improving the light-harvesting capacity and performance of cells, achieving a 13.07% initial efficiency and greatly improved current output of a-Si:H single-junction solar cell based on this architecture. Given the unique transparency characteristics of thin-film solar cells, this proposed architecture has great potential for integration into the windows of buildings, microelectronics and other applications requiring transparent components.

The particular properties of thin-film photovoltaic cells in terms of the abundance and low cost of their constituent elements, their sensitivity to low light and the maturity of manufacturing technology makes them an interesting option for low-cost solar energy production through the integration of photoelectric conversion units into everyday living. However, the greatly reduced device thickness compared to their crystalline counterpart creates a need for an effective light trapping strategy to enhance the light absorption inside the device. This has subsequently led to a number of methods being proposed based on: conventional random textured surfaces<sup>1–3</sup>, photonic crystals<sup>4–5</sup>, nanowires<sup>6–8</sup>, gratings<sup>9–11</sup>, plasmonic nanostructures<sup>12–14</sup>, back reflectors<sup>15–17</sup>, anti-reflection coatings<sup>18–21</sup> and Mie resonators<sup>22–23</sup>. All of these approaches have made good use of the solar cell spectrum and resulted in higher energy yield through an extension of the light path, but this is subject to the angular distribution of light scattered by the surface morphology. That is, incoming light can still escape from the cell's effective absorption region if it penetrates the front or back of the cell with an escape angle<sup>24</sup> greater than the total internal reflection, thereby causing an undesirable out-coupling of light into inactive absorbers around the cell.

Vertical trapping of escaped light has been achieved through the excitation of guided-mode resonances in absorbers placed between tuned interface textures<sup>25–26</sup>, which subsequently enhances absorption in the weakly absorbing region<sup>2,25–28</sup>. Lateral trapping and the in-coupling of light from the cell's adjacent regions, on the other hand, has not received the same level of consideration, even though a high out-coupling of light can further enhance absorption in the effective area. There is therefore clearly a need for new cell structure designs and light trapping concepts capable of almost complete light absorption in the weak absorbing region. To this end, this study presents a novel design based on numerical simulation for a lateral light trapping architecture capable of capturing photons in two-dimensions, and which is therefore aimed at providing a higher electrical output than one-dimensional light-trapping strategies.

In a conventional thin-film solar cell, vertical trapping structures are surrounded with inactive absorbers that are ineffective in absorbing incident light. To overcome this limitation, we adopted a lateral trapping structure in which a vertically layered cell structure (air/glass/ZnO:B/p- $\mu\text{c-SiO}_x\text{:H}$  (10 nm)/a-Si:H (300 nm)/n- $\mu\text{c-SiO}_x\text{:H}$  (30 nm)/ZnO:B/Ag) functions as the effective light absorption region (hereafter referred to as a vertical light trapping structure, or VLTS for short) and inactive absorbers are removed to create a lateral light trapping structure (LLTS). As shown in Fig. 1, these two architectures are otherwise essentially identical, with boron-doped p-type microcrystalline silicon oxide (p- $\mu\text{c-SiO}_x\text{:H}$ ) and phosphorous-doped n-type microcrystalline silicon oxide (n- $\mu\text{c-SiO}_x\text{:H}$ ) layers forming the built-in electric field<sup>29</sup>.

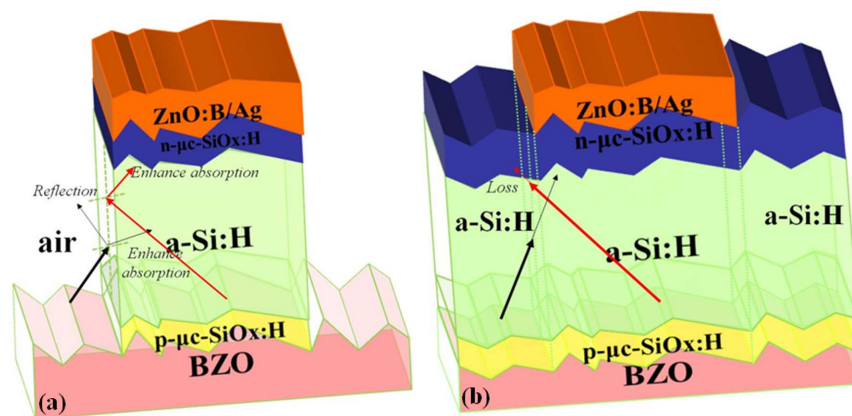


**Figure 1 | Schematic diagrams of solar cells.** (a), Schematic of LLTS. The red arrows represent light rays scattered by the marginal area between air and the a-Si:H absorber, whereas the black arrows are light rays coupled in the effective absorber from adjacent regions. The random surface morphology of the MOCVD ZnO:B substrate is represented by a wrinkled surface. (b), VLTS with inactive absorbers. The boron-doped p-type microcrystalline silicon oxide (p-μc-SiO<sub>x</sub>:H) and phosphorous-doped n-type microcrystalline silicon oxide (n-μc-SiO<sub>x</sub>:H) layers form a built-in electric field.

From a geometric optics perspective, light scattered in the effective area of the VLTS is lost from limbic regions to inactive absorbers, and any light scattered from the inactive absorbers is unlikely into the effective area due to absorption by the a-Si:H layer. In contrast, the absence of inactive absorbers in LLTS (Fig. 1a) creates a high refractive index mismatch between Si absorbers (4.8) and air (1), resulting in a reflective surface that causes laterally propagating waves to be re-reflected back into the absorber. Furthermore, scattered waves from adjacent regions propagate in the non-absorbing medium (air), which means that more light enters the cell's effective area. Thus, through careful selection of the absorption coefficient of the absorbers, this enhanced photon harvesting can also be made more effective for incident light arriving at the back reflector (ZnO:B/Ag). Subsequent simulations were therefore based on just such a scenario, in which wavelength above 500 nm were incident on an a-Si:H absorber.

To test the effectiveness of the LLTS design, the influence of lateral light trapping due to the out-coupling of light from the effective areas and the in-coupling of light from adjacent regions on the overall light absorption must be rigorously calculated by conducting the Rigorous Coupled-Wave Analysis (RCWA) simulation. The light absorption in effective areas is calculated from the divergence of the Poynting vector<sup>14</sup>:

$$Q_{\text{abs}} = \frac{1}{2} (\omega \epsilon'' |E|^2 + \omega \mu'' |H|^2) \quad (1)$$

where  $E$  and  $H$  obtained from RCWA code are the electric and magnetic fields in the a-Si:H layer, respectively;  $\omega$  is the frequency; and  $\epsilon''$  and  $\mu''$  (for a-Si:H,  $\mu'' = 0$ ) are the respective imaginary parts of the permittivity and permeability. To better illustrate the effect of the LLTS on light absorption, experimentally determined cross-sectional profiles of MOCVD deposited ZnO:B films from AFM scans were taken into account. It should be noted that a simplified vertical, but not an inhomogeneous boundary in the real case, was employed in the RCWA simulation because the photon harvesting enhancement may originate from the high refractive index mismatch between Si and air mediums and more effective absorbed light from the adjacent regions on account of the non-absorptive Air medium. In this, transverse electric (TE) polarized light with a typical wavelength of 600 nm strikes the simulated structure perpendicularly (Fig. 2a), with the resulting normalized and time-averaged electric field distributions and absorption enhancement of LLTS relative to VLTS given in Fig. 2c, d and b, respectively.

On the basis of this data, the simulated structure is divided into five regions, as indicated in Fig. 2a. Region I represents the active region

covered with ZnO:B/Ag back contact, wherein the incoming light is scattered into different directions and absorbed in the active absorber, with the resulting carriers being collected and contributing to the cell's output current. In Regions II and III, however, the absence of a back contact causes this process to collapse. Instead, elimination of the inactive absorbers (i.e., the LLTS cell shown in Fig. 3a) causes a low-angle scattering of light in Si the absorbers that increases the total internal reflection at the vertical Si/air interface between Regions I and II. Moreover, the in-coupling of light from Region II (air) can enter Region I without any additional absorption in the inactive absorbers. To fully illustrate the effective scattering range of Region II in the LLTS, the angular intensity distribution (AID) of the ZnO:B/air interface in Region II and III is shown in Fig. 3b as a function of the scattering angle and wavelength. We see from this that depending on the maximum light scattering angle in air (below 50°) of the textured, Region II is capable of coupling light that is partially scattered in Region I, and therefore contributes to the total absorption. Furthermore, even though the effective width of Region II is very nearly the same as the thickness of the absorber (about 300 nm), the region beyond this (Region III) can also couple the scattered light in Region V and create an interference that adds to the total transmission (Fig. 2c and d). Finally, in instances where no light is scattered from Region II due to the mirror effect of the ZnO:B/Ag back reflector, Region IV is found to be much darker than Region V.

As can be seen in Fig. 2b, the absorption enhancement of LLTS compared with VLTS is consistently greater than 1 across the entire weak absorbing region of a-Si:H (500–750 nm). This means that the lateral trapping and in-coupling from Region I create an out-coupling of light that generally escapes from the marginal areas, while the in-coupling of light from Region II is absorbed in the effective regions rather than the inactive absorbers.

To confirm the simulation model and the effect of LLTS on cells performance, the inactive silicon was completely removed from the cells' periphery to its front electrode by dry etching. Photographs taken of the LLTS cell (after-etching) and the VLTS cell (before-etching) (Fig. 4a and b, respectively) clearly illustrate the difference between these two structures, in that the removal of inactive silicon creates a high degree of transparency around the active area of the LLTS. It is also noted that the high transverse conductivity of doped p- or n-layers in a VLTS cell should create a transverse collecting phenomenon, in which case the carriers generated in the non-active region are collected by the adjacent active region and thereby contribute to the  $J$ - $V$  characteristics. This is similar to the horizontal transport that has been identified in polymer solar cells<sup>30</sup>, but the

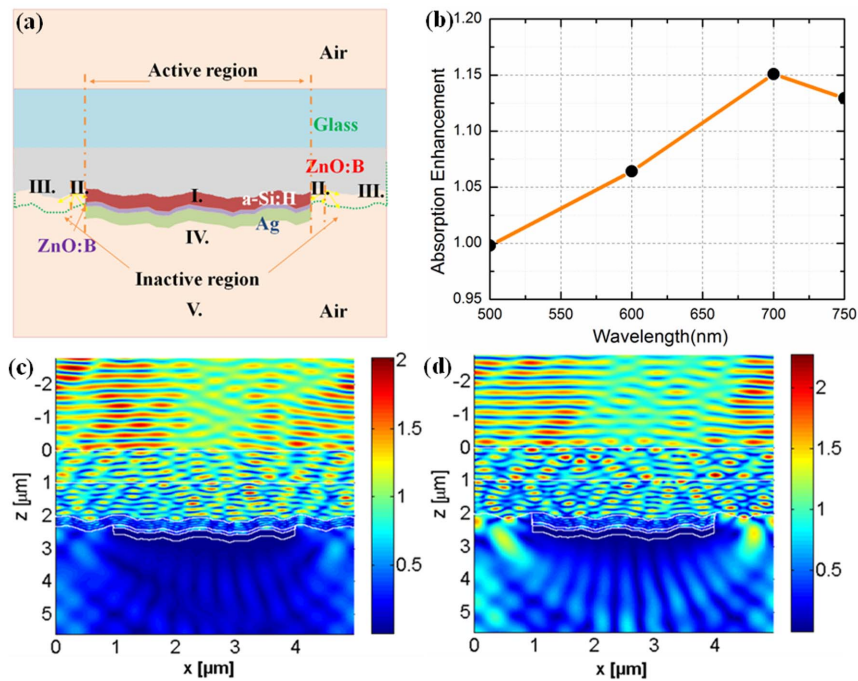


**Figure 2 | Simulation of LLTS and VLTS performance.** (a), Two-dimensional schematic of the LLTS and VLTS cells employed in RCWA code. The computational domain of the vertical layered cell structure shown in Fig. 1 was divided into five regions denoted by Roman numerals, with the zones surrounded by dashed lines indicating removed inactive absorbers. (b), Absorption enhancement of LLTS solar cells relative to VLTS versus the wavelength of light. (c), (d), Contour plot of normalized and time-averaged electric field distributions for VLTS and LLTS, respectively. The longitudinal z-axis indicates the respective layer thickness, and the horizontal x-axis represents the adopted computational domain's lateral dimension of about 5  $\mu\text{m}$ .

simultaneous enhancement of both lateral shunting and recombination loss, especially on highly textured substrates<sup>31–32</sup>, means a deterioration of electrical properties such as the open circuit voltage ( $V_{oc}$ ) and fill factor ( $FF$ ). However, the absence of this effect in the LLTS cell means that this electrical loss can be avoided.

This is confirmed by the initial  $J$ - $V$  curves of LLTS and VLTS single-junction a-Si:H solar cells (Fig. 4c), in which the LLTS shows a greatly improved  $J_{sc}$  of 21.35  $\text{mA}/\text{cm}^2$  in conjunction with a slight increase in  $V_{oc}$ . The observed decrease in  $FF$  is believed to be a consequence of damage to the cell due to plasma reactive etching. Nevertheless, an efficiency ( $Eff.$ ) gain of  $>8\%$  was achieved with the LLTS cell, with a maximum  $Eff.$  of 13.07%, being much higher than the best reported single-junction a-Si:H solar cells up to now<sup>33</sup>. Fig. 4d shows a statistical graph of the  $J_{sc}$  of the LLTS and VLTS cells,

in which the cell numbers correspond to the eight cells in Fig. 4a. This demonstrates that the LLTS cell has a higher  $J_{sc}$  at all points, thus proving the effectiveness of the design. Furthermore, these experimental results are all in good agreement with the calculation trends (see Fig. 2b).

Through this study, we have developed a light trapping strategy for harvesting the laterally propagating waves that have previously not been considered in traditional light trapping approaches. The basis of this design is also applicable to thin-film technologies other than silicon solar cells. The application of this lateral trapping concept may therefore provide new opportunities for novel photon-harvesting designs, and further performance improvements in existing technologies. Furthermore, in addition to the identified performance gain in photon harvesting, the highly transparent nature of this

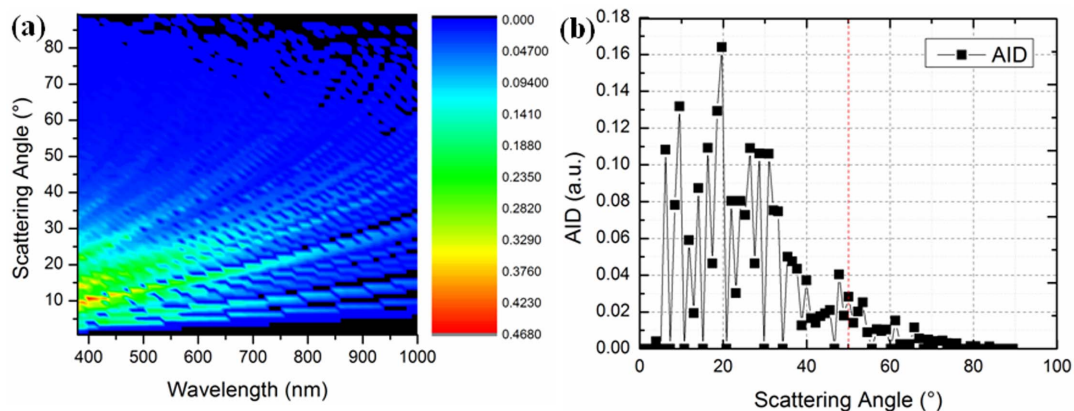


**Figure 3 | Angular intensity distribution of the ZnO:B/Air interface.** (a), Contour plot of AID (a function of the scattering angle and incident wavelength) for the ZnO:B/air interface. The colored bar provides a measure of the scattering intensity of light for a given angle and wavelength. (b), Extracted AID distribution for an incident light wavelength of 600 nm. The general cutoff scattering angle, above which no scattered light exists, is indicated by the dashed red line.



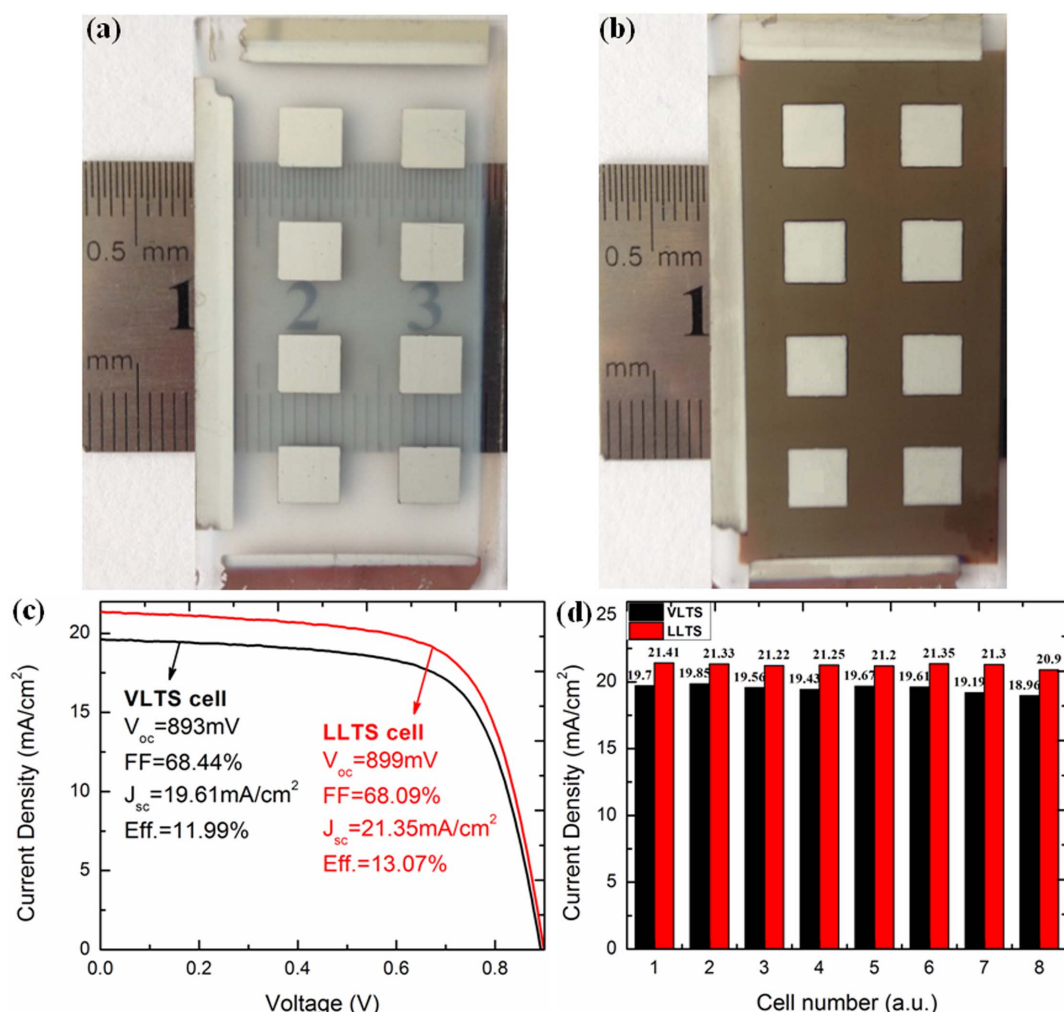


**Figure 4 | Photographs and characteristics of single-junction a-Si:H solar cells.** (a), LLTS cell (after-etching). (b), VLTS cell (before-etching). (c), Initial  $J$ - $V$  curves for the VLTS (black line) and LLTS cell (red line). (d), Statistical plot of  $J_{sc}$  for the VLTS (black) and LLTS (red) cells.

LLTS compared with traditional thin-film solar cell structures presents promising implications for integrated photovoltaics or integrated photovoltaic chargers for portable electronics.

## Methods

**Single-junction a-Si:H solar cell fabrication.** Boron-doped zinc oxides (BZO) as front electrodes were grown on glass by metal-organic chemical vapor deposition (MOCVD) with a root mean square roughness and sheet resistance of 80 nm and 25  $\Omega/\text{sq}^{-1}$ , respectively. Subsequently, boron-doped hydrogenated microcrystalline silicon oxide (p- $\mu\text{c-SiO}_x\text{:H}$ ) window layer with a thickness of 12 nm was deposited on BZO. Then, hydrogenated intrinsic amorphous silicon oxide layer was inserted between this p-layer and a 300 nm thick hydrogenated intrinsic amorphous silicon layer (i-a-Si:H) as a p/i buffer layer. Phosphorus-doped  $\mu\text{c-SiO}_x\text{:H}$  layer was then deposited directly onto the i-a-Si:H layer, thus forming a built-in potential with the p-layer. Finally, in order to enhance the absorption, BZO/Ag layer was applied as a back reflection electrode. The active area of the cells was 0.253  $\text{cm}^2$ .

All of the silicon thin films were deposited by radio frequency plasma-enhanced chemical vapor deposition (RF-PECVD) using a substrate temperature of 210°C. Sulfur hexafluoride ( $\text{SF}_6$ ) was used as the etchant gas to remove silicon from the cell by dry etching at a power density and pressure of 750  $\text{W}/\text{cm}^2$  and 70 Pa, respectively.

**Solar cell characterization.** The current-voltage ( $J$ - $V$ ) characteristics were measured under standard conditions (AM1.5, 100  $\text{mW}/\text{cm}^2$ ) at 25°C using a dual-lamp solar simulator (WXS-156S-L2, AM 1.5 GMM).

- Battaglia, C. *et al.* Nanomoulding of transparent zinc oxide electrodes for efficient light trapping in solar cells. *Nature Photon.* **5**, 535–538 (2011).
- Battaglia, C. *et al.* Light Trapping in Solar Cells: Can Periodic Beat Random? *ACS Nano* **6**, 2790–2797 (2012).

- Battaglia, C. *et al.* Nanoimprint Lithography for High-Efficiency Thin-Film Silicon Solar Cells. *Nano Lett.* **11**, 661–665 (2011).
- Park, Y. *et al.* Absorption enhancement using photonic crystals for silicon thin film solar cells. *Opt. Express* **17**, 14312–14321 (2009).
- Zeng, L. *et al.* Efficiency enhancement in Si solar cells by textured photonic crystal back reflector. *Appl. Phys. Lett.* **89**, 111111 (2006).
- Garnett, E. & Yang, P. Light Trapping in Silicon Nanowire Solar Cells. *Nano Lett.* **10**, 1082–1087 (2010).
- Peng, K. Q. & Lee, S. T. Silicon Nanowires for Photovoltaic Solar Energy Conversion. *Adv. Mater.* **23**, 198–215 (2011).
- Tang, J., Huo, Z., Brittman, S., Gao, H. & Yang, P. Solution-processed core-shell nanowires for efficient photovoltaic cells. *Nat. Nanotech.* **6**, 568–572 (2011).
- Yu, Z., Raman, A. & Fan, S. Fundamental Limit of Light Trapping in Grating Structures. *Opt. Express* **18**, A366–A380 (2010).
- Peters, M., Rüdiger, M., Hauser, H., Hermle, M. & Bläsi, B. Diffractive gratings for crystalline silicon solar cells—optimum parameters and loss mechanisms. *Prog. Photovolt: Res. Appl.* **20**, 862–873 (2012).
- Haase, C. & Stiebig, H. Optical Properties of Thin-film Silicon Solar Cells with Grating Couplers. *Prog. Photovolt: Res. Appl.* **14**, 629–641 (2006).
- Tan, H., Santbergen, R., Smets, Arno, H. M. & Zeman, M. Plasmonic Light Trapping in Thin-film Silicon Solar Cells with Improved Self-Assembled Silver Nanoparticles. *Nano Lett.* **12**, 4070–4076 (2012).
- Atwater, H. A. & Polman, A. Plasmonics for improved photovoltaic devices. *Nat. Mater.* **9**, 205–213 (2010).
- Ferry, V. E., Polman, A. & Atwater, H. A. Modeling Light Trapping in Nanostructured Solar Cells. *ACS Nano* **5**, 10055–10064 (2011).
- O'Brien, P. G. *et al.* Silicon Photovoltaics Using Conducting Photonic Crystal Back-Reflectors. *Adv. Mater.* **20**, 1577–1582 (2008).
- Söderström, K. *et al.* UV-nano-imprint lithography technique for the replication of back reflectors for n-i-p thin film silicon solar cells. *Prog. Photovolt: Res. Appl.* **19**, 202–210 (2011).



17. Cao, W. *et al.* Enhancing Light Harvesting in Organic Solar Cells with Pyramidal Rear Reflectors. *Appl. Phys. Lett.* **99**, 023306 (2011).
18. Zhu, J. *et al.* Optical Absorption Enhancement in Amorphous Silicon Nanowire and Nanocone Arrays. *Nano Lett.* **9**, 279–282 (2009).
19. Chyan, J. Y., Hsu, W. C. & Yeh, J. A. Broadband antireflective poly-Si nanosponge for thin film solar cells. *Opt. Express* **17**, 4646–4651 (2009).
20. Min, W. L., Jiang, B. & Jiang, P. Bioinspired Self-Cleaning Antireflection Coatings. *Adv. Mater.* **20**, 3914–3918 (2008).
21. Wang, K. X., Yu, Z., Liu, V., Cui, Y. & Fan, S. Absorption Enhancement in Ultrathin Crystalline Silicon Solar Cells with Antireflection and Light-Trapping Nanocone Gratings. *Nano Lett.* **12**, 1616–1619 (2012).
22. Spinelli, P., Verschuuren, M. A. & Polman, A. Broadband omnidirectional antireflection coating based on subwavelength surface Mie resonators. *Nat. Commun.* **3**, 692 (2012).
23. Ferry, V. E. *et al.* Optimized Spatial Correlations for Broadband Light Trapping Nanopatterns in High Efficiency Ultrathin Film a-Si:H Solar Cells. *Nano Lett.* **11**, 4239–4245 (2011).
24. Haasea, C. & Stiebig, H. Thin-film silicon solar cells with efficient periodic light trapping texture. *Appl. Phys. Lett.* **91**, 061116 (2007).
25. Haug, F.-J., Söderström, T., Cubero, O., Daudrix, V. T. & Ballif, C. Influence of the ZnO buffer on the guided mode structure in Si/ZnO/Ag multilayers. *J. Appl. Phys.* **106**, 044502 (2009).
26. Haug, F.-J., Söderström, K., Naqavi, A. & Ballif, C. Resonances and absorption enhancement in thin film silicon solar cells with periodic interface texture. *J. Appl. Phys.* **109**, 084516 (2011).
27. Söderström, K., Haug, F.-J., Escarré, J., Cubero, O. & Ballif, C. Photocurrent Increase in n-i-p Thin Film Silicon Solar Cells by Guided Mode Excitation via Grating Coupler. *Appl. Phys. Lett.* **96**, 213508 (2010).
28. Lee, Y., Huang, C., Chang, J. & Wu, M. Enhanced light trapping based on guided mode resonance effect for thin-film silicon solar cells with two filling-factor gratings. *Opt. Express* **16**, 7969–7975 (2008).
29. Fang, J. *et al.* Improvement in performance of hydrogenated amorphous silicon solar cells with hydrogenated intrinsic amorphous silicon oxide p/i buffer layers. *Sol. Energy Mater. Sol. Cells* **128**, 394–398 (2014).
30. Anshuman, J. & Das, K. S. Narayan. Retention of power conversion efficiency from small area to large area polymer solar cells. *Adv. Mater.* **25**, 2193–2199 (2013).
31. Lambertz, A., Grundler, T. & Finger, F. Hydrogenated amorphous silicon oxide containing a microcrystalline silicon phase and usage as an intermediate reflector in thin-film silicon solar cells. *J. Appl. Phys.* **109**, 113109 (2011).
32. Buehlmann, P. *et al.* In situ silicon oxide based intermediate reflector for thin-film silicon micromorph solar cells. *Appl. Phys. Lett.* **91**, 143505 (2007).
33. Benagli, S. *et al.* High-efficiency amorphous silicon devices on LPCVD-ZNO TCO prepared in industrial KAI-M R&D reactor. 24th European Photovoltaic Solar Energy Conference, Hamburg (2009).

## Acknowledgments

We are grateful for financial support from the National Basic Research Program of China (Grant Nos. 2011CBA00706), Science and Technology Support Program in Tianjin (12ZCZDZX03600), Major Science and Technology Support Project of Tianjin City (No. 11TXXSYGX22100), and Specialized Research Fund for the PhD Program of Higher Education (20120031110039).

## Author contributions

X.Z., J.F. and B.L. conceived the study. J.F. carried out the experiment. B.L. carried out the computations. J.F., B.L. and X.Z. wrote the manuscript. J.F., B.L., Y.Z. and X.Z. discussed the results.

## Additional information

**Competing financial interests:** The authors declare no competing financial interests.

**How to cite this article:** Fang, J., Liu, B., Zhao, Y. & Zhang, X. Two-dimensional high efficiency thin-film silicon solar cells with a lateral light trapping architecture. *Sci. Rep.* **4**, 6169; DOI:10.1038/srep06169 (2014).



This work is licensed under a Creative Commons Attribution-NonCommercial-NoDerivs 4.0 International License. The images or other third party material in this article are included in the article's Creative Commons license, unless indicated otherwise in the credit line; if the material is not included under the Creative Commons license, users will need to obtain permission from the license holder in order to reproduce the material. To view a copy of this license, visit <http://creativecommons.org/licenses/by-nc-nd/4.0/>